Article

Monitoring of Trace Gases over Antarctic by GaoFen-5/AIUS: Algorithm Description and First Retrieval Results of O_3 , H_2O and HCl

Xiaoying Li[1,*], Tianhai Cheng[1], Jian Xu[2,*], Hailiang Shi[3], Pengmei Xu[4], Xingying Zhang[5], Shule Ge[6], Hongmei Wang[1], Songyan Zhu[6], Jing Miao[1] and Qi Luo[1]

1. State Key Laboratory of Remote Sensing Science, Institute of Remote Sensing and Digital Earth, Chinese Academy of Sciences, Beijing 100101, China; lixy01@radi.ac.cn (X.L.)
2. Remote Sensing Technology Institute, German Aerospace Center (DLR), Oberpfaffenhofen, Germany
3. Anhui Institute of Optics and Fine Mechanics, Chinese Academy of Sciences, Hefei, Anhui, 230031, China
4. Beijing Institute of Space Mechanics & Electricity, Beijing 100094, China;
5. National Satellite Meteorological Center, China Meteorological Administration
6. China Center for Resources Satellite Data and Application, China

* Correspondence: lixy01@radi.ac.cn (X.L.), jian.xu@dlr.de (J.X.)

Abstract: AIUS (Atmospheric Infrared Ultraspectral Sounder) is an infrared occultation spectrometer onboard the Chinese GaoFen-5 satellite, which covers a spectral range of 2.4--13.3 μm (750--4100 cm^{-1}) with a spectral resolution of about 0.02 cm^{-1}. AIUS was designed to measure and to study chemical processes of ozone (O_3) and other trace gases in the upper troposphere and stratosphere over Antarctic. In this study, the corresponding retrieval methodology is described. The comparison between AIUS measurements and simulated spectra illustrates that AIUS measurements agree well to the simulated spectra. To first evaluate the reliability of our retrieval algorithm, three retrieval O_3 experiments are performed based on ACE-FTS observation spectra. A comparison between our retrieved profiles and the ACE-FTS official products shows that the relative difference of these three retrieval experiments is mostly within 10% between 20 km and 70 km. These retrieval experiments demonstrate that the retrieval algorithm described in this study work fine and reliable. Furthermore, O_3, H_2O and HCl profiles are retrieved from eight orbits of AIUS measurements and compared with the official AURA/MLS level-2 v4.2 profiles. Comparison experiments show that the relative difference is mostly within 10% (about 0.02 - 0.4 ppm) between 18 and 58 km for O_3 retrieval, within 10% (0-0.5 ppm) between 15 and 80 km for H_2O retrieval, and within 10% (about 0.1 ppb) between 30 and 60 km for HCl retrieval. There is a good agreement in the retrieved trace gas profiles obtained from AIUS and from coincident profiles from MLS.

Keywords: AIUS; occultation; retrieval algorithm; microwindows; ozone

1. Introduction

The annual occurrence of the Antarctic ozone hole has been well documented. For studying ozone recovery, many efforts have been made to understand the chemical and dynamical processes around Antarctic [1-3]. Occultation and limb sounding techniques have provided an important way for remotely observing Earth's middle atmosphere. These measurements have greatly promoted our understanding of the chemical process of atmospheric composition in the upper troposphere and stratosphere by providing profile measurements with different altitudes. As compared to nadir-viewing measurements, occultation/limb sounding measurements have higher vertical resolution, which can be used to derive vertical information of atmospheric components. Furthermore, high-resolution atmospheric mid-infrared spectra are suitable for detection of many trace species, since a wide variety of vibrational-rotational bands with molecular absorption lines are found within this spectral range. Recently, many occultation observation/limb sounding sensors

Preprints (www.preprints.org) | NOT PEER-REVIEWED | Posted: 26 June 2019 doi:10.20944/preprints201906.0257.v1

have been developed and provided abundant profiles of trace gases, such as O_3, CO, H_2O, NO, etc [4-9].

AIUS is one of six payloads onboard the Chinese GaoFen-5 satellite which has been launched successfully on May 9, 2018 (Beijing local time). AIUS is the first occultation spectrometer developed in China, with the aim of detecting the trace gases over the Antarctic. AIUS operates in a solar synchronous orbit, with a nominal height of 705 km. The instrument is a Fourier transform infrared spectrometer and its main objective is to measure the O_3 and other species in the stratosphere and upper troposphere in order to study the ozone temporal variations over the Antarctic.

The main objective of this paper is to introduce the trace gas retrieval algorithm developed for AIUS and to discuss the first results of O3, H2O and HCl retrieval from AIUS. In Section 2, the AIUS instrument and the corresponding measurement characteristics are presented. Section 3 describes the retrieval methodology including the employed inversion algorithm, selection of fitting windows and the integrated atmospheric profiles in detail. In Section 4, ACE-FTS measurements are used to retrieve O_3 profiles to assess the retrieval algorithm. Then, O_3, H_2O and HCl profiles retrieved from AIUS measurements are compared with MLS products.

2. AIUS instrument and measurements

2.1. Instrument

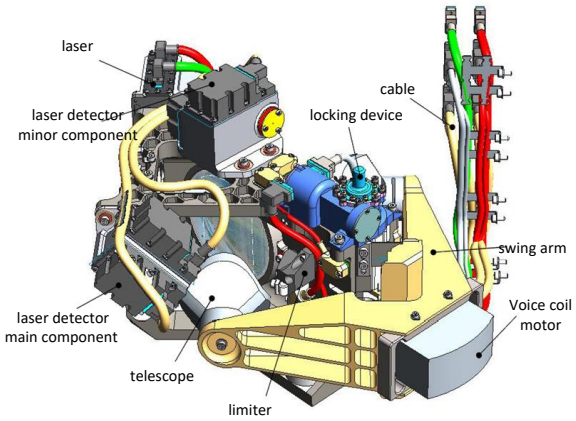

Figure 1 AIUS interferometer model [10]

AIUS is a Fourier transform infrared spectrometer for the detection of occultation transmittance spectra in the middle and upper atmosphere. Its interferometer model is depicted in Figure 1. AIUS has characteristics similar to those of ACE-FTS. Both instruments have a spectral resolution of 0.02 cm^{-1}. AIUS covers a spectral range from 750 cm^{-1} to 4100 cm^{-1}, while ACE-FTS covers 750--4400 cm^{-1}. AIUS is a dual-band system composed of MCT (mercury cadmium telluride, 750--1850 cm^{-1}) and InSb (1850--4160 cm^{-1}). The instrument covers an altitude range from 8 to 100 km and has a field of view (FOV) of 1.25 mrad. A brief description of the two instruments is shown in Table 1 [11-12].

Table 1 Instrument characteristics of GaoFen5-AIUS and ACE-FTS

Parameters	**AIUS**	**ACE-FTS**
Orbit inclination	98.218°	74°
Orbit altitude	705 km	650 km
Observation mode	Solar occultation	Solar occultation
Spectra range	750~4100 cm^{-1}	750~4400 cm^{-1}
spectra resolution	0.02 cm^{-1}	0.02 cm^{-1}
Field of view (FOV)	1.25mrad	1.25mrad
Signal Noise Ratio	1000-2000 cm^{-1}: 200-350	>300 over most of the

Preprints (www.preprints.org) | NOT PEER-REVIEWED | Posted: 26 June 2019 doi:10.20944/preprints201906.0257.v1

(SNR)	2000-3200 cm^{-1}: >300 other spectral bands: 100-200	spectral band

AIUS obtains measurements of atmospheric parameters remotely by recording solar transmittance spectra as it is tracking the sun and scanning through the atmosphere (see Figure 2). The sun tracking is fulfilled by the sun tracking camera. The center position of the sun is acquired by real-time processing of the sun tracking image, which is fed back to the two-dimensional pointing mechanism, and the pointing mechanism is adjusted so that the central field of view of the detector always points to the center position of the sun. The uncertainty of sun tracking is within 25 μrad [10].

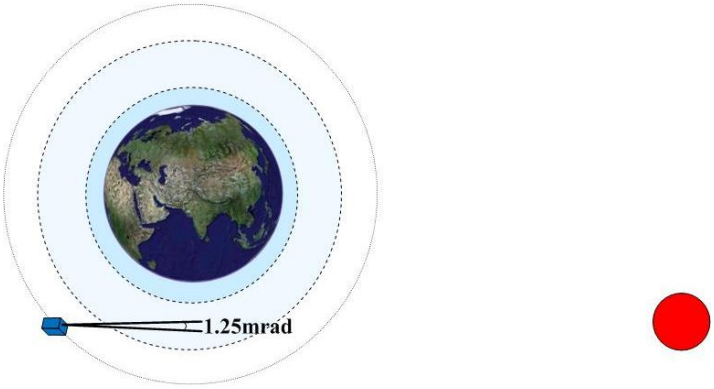

Figure 2 AIUS measurement geometry

AIUS travels in a sun-synchronous orbit and observes in a forward direction with a deviation angle from the along track orbit. The deviation angle varies between 0 and 25°. The occultation spectra are scanned in an upward direction from the time of the sun rising above the horizon to the time of the sun moving out of the atmosphere. It takes 2 seconds in every scan at one tangent point and takes about 3 minutes for a scan sequence from the lowest altitude (about 8 km) to the highest altitude (about 100 km) in the atmosphere. Then, it detects the solar spectra outside the atmosphere. Subsequently, the pointing mirror points to the deep space for producing the cold reference, which is used to calibrate the systematic errors. The measurements are repeated for each sunrise. AIUS measurements are mainly over the Antarctic. Figure 3 shows that the latitude coverage of AIUS is between 55°S and 90°S.

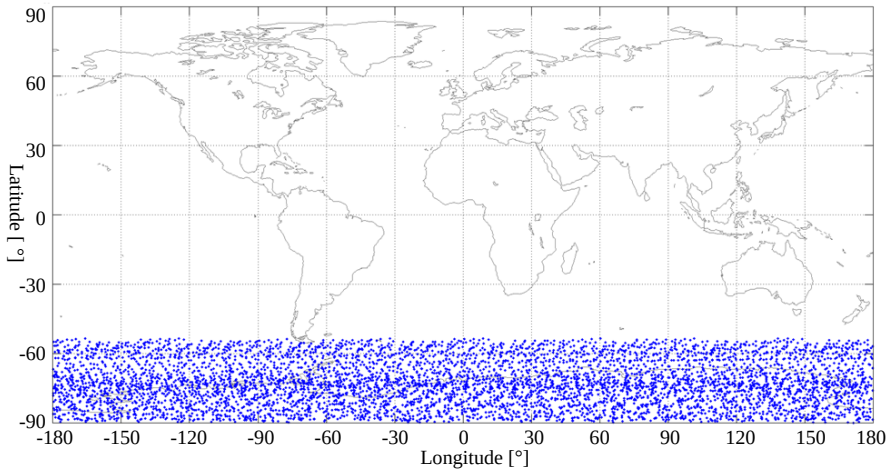

Figure 3 The coverage of AIUS measurements

2.2. Measurement spectra

Preprints (www.preprints.org) | NOT PEER-REVIEWED | Posted: 26 June 2019 doi:10.20944/preprints201906.0257.v1

The GF5-AIUS level 0 data is original auxiliary and interferogram data in a binary format. The level 1 data is stored in HDF5 files including reconstructed spectra and processed auxiliary data. The AIUS level 0 -1 processing includes four steps. The first step is the acquisition and processing of auxiliary data. By unpacketizing the auxiliary data package, information such as acquisition time, sun position and satellite position, is acquired. The geometric parameters, the height and the latitude and longitude coordinates, are calculated from the information of the sun and satellite. The second step is to reconstruct the spectra from the original interferogram. However, due to its instrument properties, the observed spectra can be contaminated by spikes that are related to the effect of energetic particles from space electromagnetic environment on orbits. The spikes removal is considered in level 1 processing. The nonlinear behavior of the detectors is expected. This nonlinearity correction has been consolidated in-flight using commissioning phase data. After that, the FFT (Fast Fourier Transformation) is performed to compute the spectra. The third step is to evaluate the spectra's quality by standard deviation or mean value of imaginary part of the calculated spectra by adding an additional quality flag.

The last step of level 1 processing is to calculate transmittance, which is directly acquire from DN (digital number) values. In addition to the observation of the Sun outside and inside the atmosphere, GF5-AIUS also observes the deep space to remove the instrumental emission. Commonly, the transmittance $\boldsymbol{\tau}(h,\lambda)$ at tangent point h can be calculated by the following equation:

$$\boldsymbol{\tau}(h,\lambda) = \frac{\boldsymbol{D}(h,\lambda)-\boldsymbol{B}(\lambda)}{\boldsymbol{S}(\lambda)-\boldsymbol{B}(\lambda)}, \quad (1)$$

where $\boldsymbol{D}(h,\lambda)$, $\boldsymbol{S}(\lambda)$ and $\boldsymbol{B}(\lambda)$ are the digital counts of the observation of signal at tangent point h, the solar radiation outside atmosphere and the deep space signal.

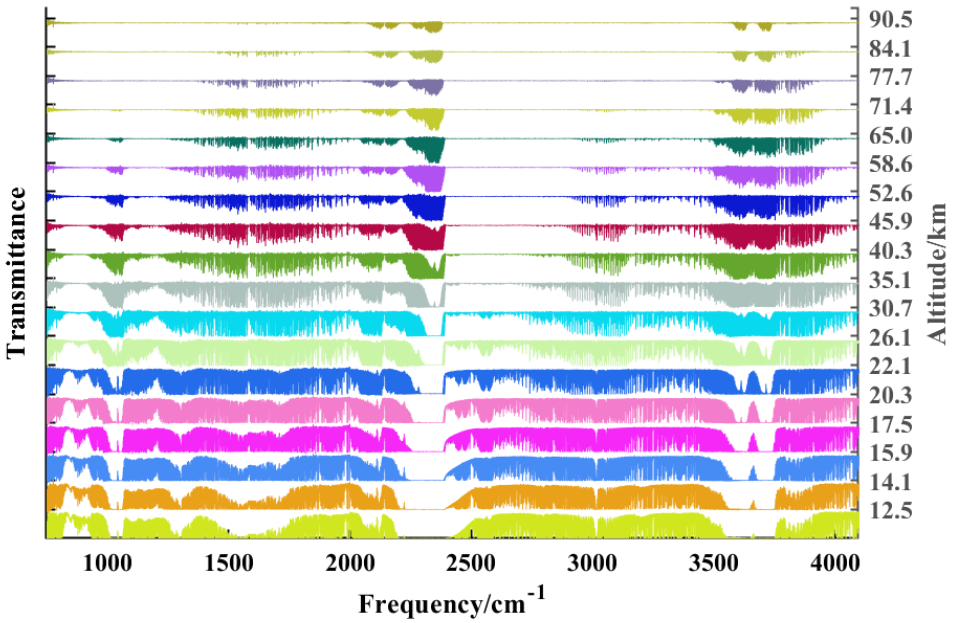

Figure 4 AIUS measurements spectra at 64.7°S142.5°W on January 8, 2019

After about seven months of on-orbit test, AIUS have been providing measurement spectra. Figure 4 shows AIUS spectra observed on January 8, 2019. To have a deeper understanding of the quality of AIUS measurement spectra, we compare the AIUS measurements with the simulated spectra. The atmospheric profiles used in the simulation are adopted from the integrated atmospheric profiles which will be described in Section 3.3. Figure 5 presents the comparison in the range of 1000-1200 cm^{-1}, 1400-1600 cm^{-1} and 2800-3000 cm^{-1}, which mainly contain the retrieval windows for O_3, H_2O and HCl respectively. Figure 5(a) show the comparison between 1000 cm^{-1} and 1200 cm^{-1} at 33.4 km. Figure 5(b)-(c) show the spectra between 1400 cm^{-1} and 1600 cm^{-1} at 18.6 km and between 2800 cm^{-1} and 3000 cm^{-1} at 26.1 km. The zoom in windows clearly illustrates that AIUS measurement spectra agree well with the simulated spectra.

Preprints (www.preprints.org) | NOT PEER-REVIEWED | Posted: 26 June 2019 doi:10.20944/preprints201906.0257.v1

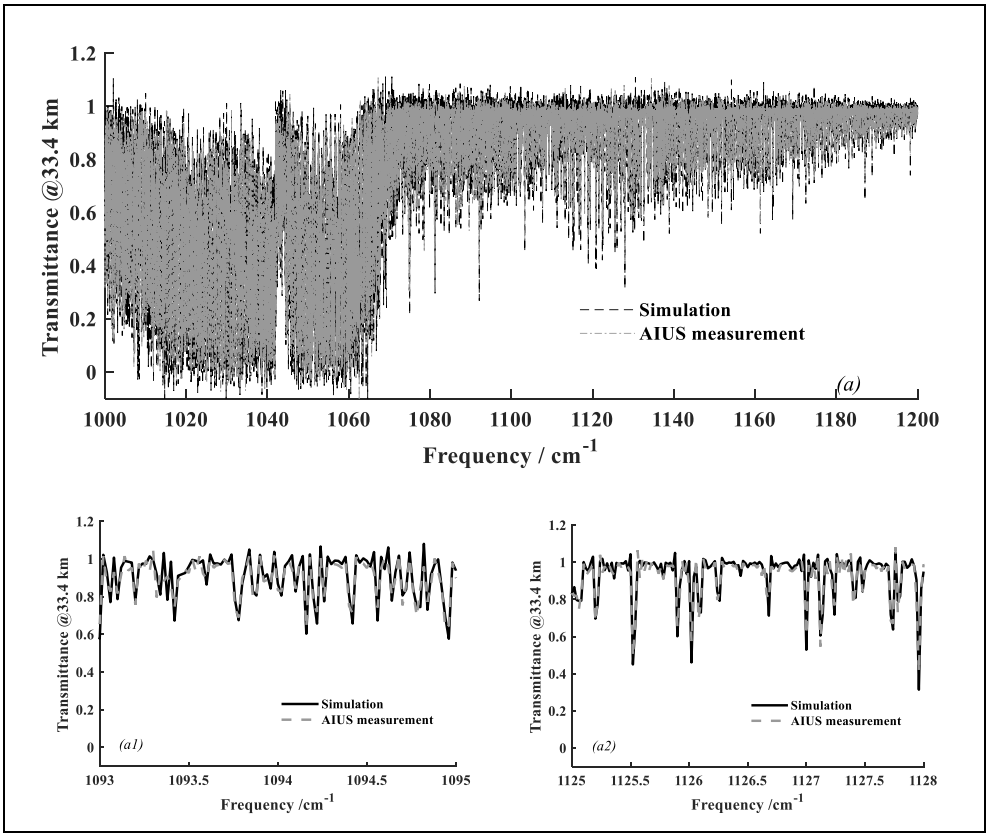

129 (a)

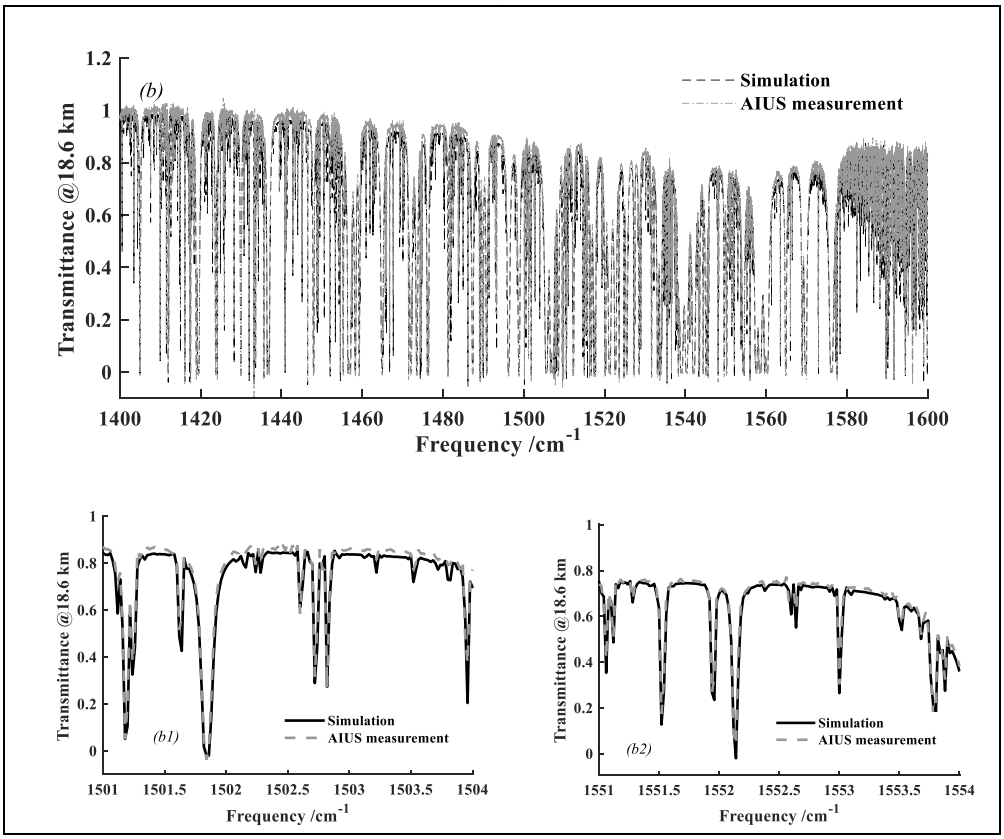

130 (b)

Preprints (www.preprints.org) | NOT PEER-REVIEWED | Posted: 26 June 2019 doi:10.20944/preprints201906.0257.v1

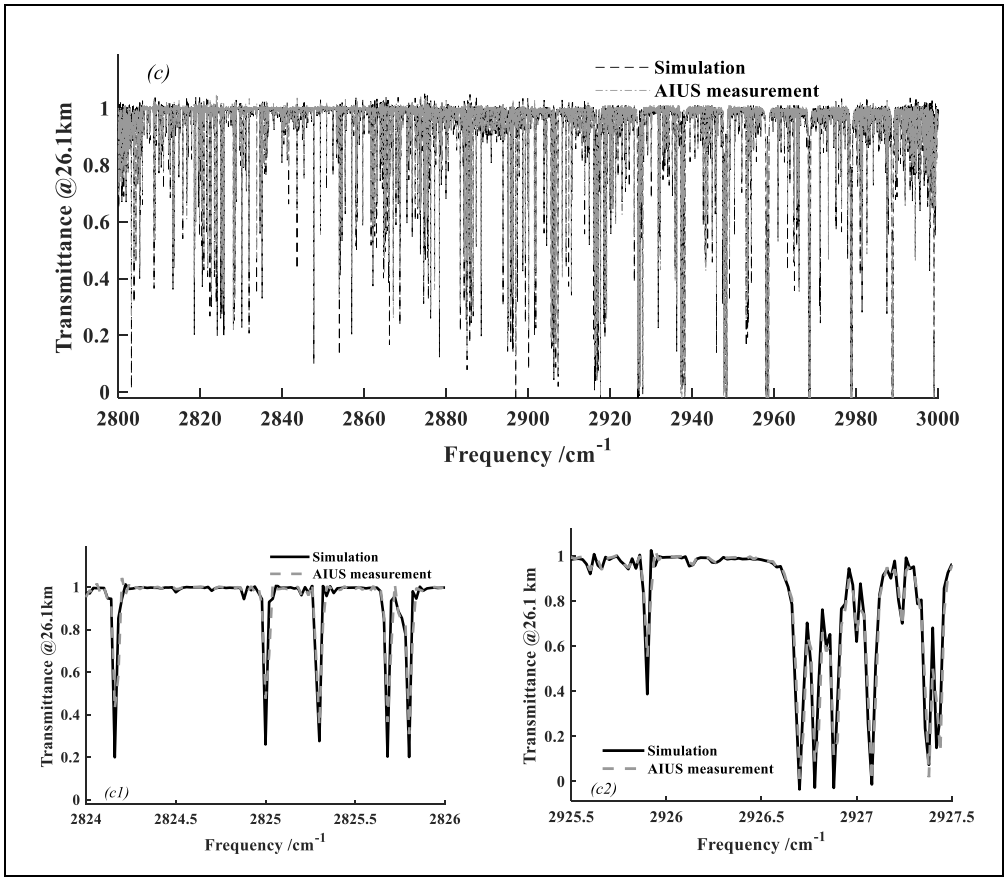

(c)

Figure 5 The comparison between AIUS measurement spectra and the simulated spectra. (a) Spectra (1000-1200 cm^{-1}) at 63.5°S6.9°E on January 1, 2019; (b) Spectra (1400-1600 cm^{-1}) at 63°S80°W on December 21, 2018; (c) Spectra (2800-3000 cm^{-1}) at 64.7°S142.48°W on January 1, 2019.

3. Retrieval methodology of AIUS

Accurate knowledge of pointing and *p*/*T* information is important to high-precision quantitative retrieval of abundances of atmospheric species from occultation observed transmittances. The tangent height correction for AIUS is carried out by employing the triangular iteration with tangential strides technique in a microwindow of N_2 continuum absorption. Details of the design and development of the tangent height correction algorithms are introduced in other paper [13]. Details about the *p*/*T* retrieval will be introduced in our future paper about validation of *T* profiles.

3.1. Inversion model

An accurate modelling of the radiative transfer through the atmosphere plays an important role in the inversion. The forward model adopted in the retrieval algorithm of AIUS is the RFM (Reference Forward Model) [14] (Dudhia, A. 2017) with the latest release version v4.36 (http://eodg.atm.ox.ac.uk/RFM/ index.html). Von Clarmann et al. [15] have compared five forward models including the RFM. The inter-comparison experiment showed that an overall agreement between all models was reached, and RFM is proven to produce reliable simulations.

The inversion algorithm employed in this study is based on OEM (Optimal Estimation Method) proposed by Rodgers [16]. The OEM retrieval framework has been widely applied to inversion of atmospheric state parameters using infrared and microwave remote sensing measurements, with nadir, occultation or limb viewing [17-22]. OEM stabilizes the inversion process by taking into account the statistical information about the atmospheric variability, which has been investigated by many studies [23-29].

Preprints (www.preprints.org) | NOT PEER-REVIEWED | Posted: 26 June 2019 doi:10.20944/preprints201906.0257.v1

Our inversion scheme uses LM (Levenberg--Marquardt) method for solving the underlying least-squares fitting problem. By introducing a constraint factor γ, the next iterate is yielded by:

$$\boldsymbol{X}_{i+1} = \boldsymbol{X}_i + [(1+\gamma)\mathbf{S}_a^{-1} + \mathbf{K}_i^T\mathbf{S}_e^{-1}\mathbf{K}_i]^{-1} \cdot \{\mathbf{K}_i^T\mathbf{S}_e^{-1}[\boldsymbol{Y} - \boldsymbol{F}(X)] - \mathbf{S}_a^{-1}[\boldsymbol{X}_i - \boldsymbol{X}_a]\}. \quad (2)$$

The inverse of the solution covariance in equation (2) is given by:

$$\mathbf{S}_x^{-1} = \mathbf{S}_a^{-1} + \mathbf{K}^T\mathbf{S}_e^{-1}\mathbf{K} \ . \quad (3)$$

And the cost function $C(\boldsymbol{X})$ is given by:

$$C(\boldsymbol{X}) = [(\boldsymbol{Y} - \boldsymbol{F}(X))^T\mathbf{S}_e^{-1}(\boldsymbol{Y} - \boldsymbol{F}(X)) + (\boldsymbol{X} - \boldsymbol{X}_a)^T\mathbf{S}_a^{-1}(\boldsymbol{X} - \boldsymbol{X}_a)]/n_y \ , \quad (4)$$

where $\boldsymbol{F}$ is the forward model, $\boldsymbol{Y}$ is a vector of observations, $\boldsymbol{X}$ is the state of the atmosphere, $\mathbf{S}_e$ is the covariance matrix of the observation error and $\mathbf{K}$ is the matrix of weighting function. The a priori state vector is denoted by $\boldsymbol{X}_a$, with its covariance matrix $\mathbf{S}_a$. n_y is the length of $\boldsymbol{Y}$ vector.

In our retrieval scheme, we have fully taken into account the characteristics of AIUS when deciding the factor γ and the covariance matrix $\mathbf{S}_a$. Firstly, retrieval experiments are made based on many simulated spectra and AIUS observation data to decide an optimal γ. After statistical analysis, the factor of γ is defined as a linear scaled function to the cost function and is updated at each iteration:

$$\gamma_i = a/C(\boldsymbol{X}_i) \ . \quad (5)$$

where a is a constant is a constant variable and changes for different atmospheric species.

The definition of the a priori covariance matrix $\mathbf{S}_a$ follows Gaussian statistics and considers the correlation between different components of the state vector and the forward model vector [30]. Different types of the correlation function [30] for computing the correlation have been tested based on the AIUS measurement spectra. In this study, we employ the linear correlation function:

$$\mathbf{S}_a(i,j) = \max\{0, \sigma(i)\sigma(j)\left[1 - (1-e^{-1})\frac{2|z(i)-z(j)|}{l_c(i)-l_c(j)}\right]\} \ , \quad (6)$$

where i and j are position indexes, z is the position, lc is the correlation length and $|*|$ signifies the absolute value. σ is the standard deviation calculated from the a priori.

3.2 Spectral microwindows of O_3, H_2O and HCl

The spectral resolution of AIUS is about 0.02 cm^{-1}. Because of this, the number of data points from each absorption band becomes unrealistic for an efficient inversion process. Furthermore, one should avoid the effect of interfering species on the retrieval of the target species and have the best information on the retrieval. Thus, the retrieval is performed using a set of narrow spectral interval (called "microwindow") instead of an entire spectral band.

To select an appropriate set of microwindows, a sensitivity analysis with Jacobians is required. First of all, we select the spectral points which are sensitive to the target gas on each cutting height and are not sensitive to the interference gas according to the Jacobians of target and the interference species. Then, the selected spectral points are increased on the basis of information entropy to generate a series of continuous window [31]. Finally, all the selected spectral microwindows at every tangent height are combined.

Spectral microwindow selection for the retrieval of O_3, H_2O and HCl are performed. Figure 6 shows the selected microwindows for O_3, H_2O, and HCl retrievals, respectively. For O_3 retrieval, about 15 spectral microwindows are selected, covering from 5 km to 95 km. Microwindows of 1020--1070 cm^{-1} are sensitive at higher altitudes, while others are sensitive at lower altitudes. About 13 spectral microwindows are selected for H_2O retrievel between 1200 and1700 cm^{-1}, covering from 8 km to 100 km. Two spectral microwindows locate between 1200 and 1250 cm^{-1}, 11 microwindows locate between 1400 and1600 cm^{-1}. About 8 spectral microwindow covering from 8 km to 85 km are selected for HCl, mainly distribute between 2800 and 3000 cm^{-1}. The microwindows for each retrieval target contains about 150-200 spectral points.

Preprints (www.preprints.org) | NOT PEER-REVIEWED | Posted: 26 June 2019 doi:10.20944/preprints201906.0257.v1

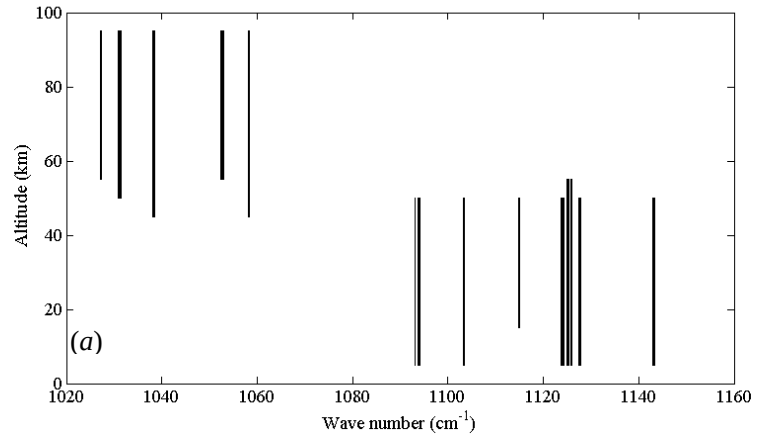

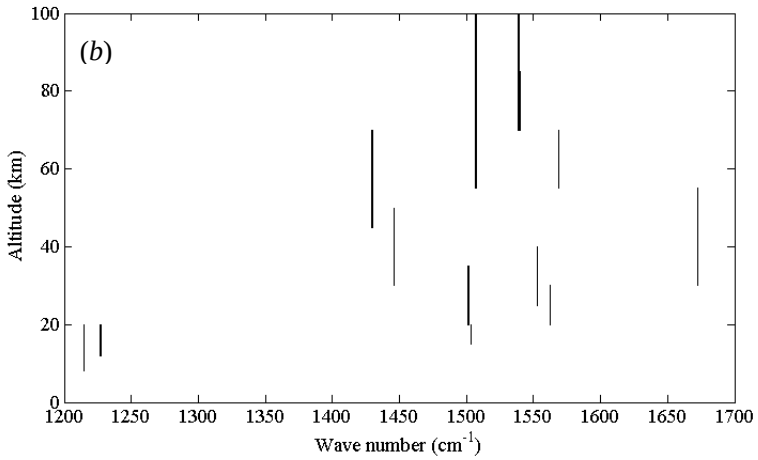

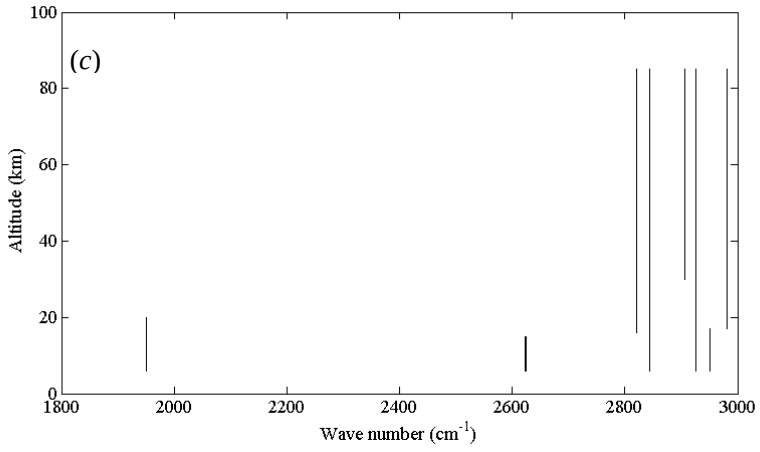

Figure 6 The spectral microwindows. (a) O_3 (b) H_2O (c)HCl

3.3 Integrated Atmospheric profiles

The forward model generates a numerical simulation of measurements based on the given atmospheric state. In other words, the accuracy of the simulated measurements depends on the reliability of the atmospheric parameters used in the forward model. In our retrieval scheme, we compute a dataset of integrated atmospheric profiles based on MLS (Microwave Limb Sounder) level 2 products, ACE-FTS Climatology-Version 3.5 and the profiles from AFGL(Air Force Geophysics Laboratory) atmospheric models.

The MLS level 2 (v4.2) products between 2014 and 2016 are considered. We classify and store the species profiles month by month for each set of products. Then, the monthly mean profiles are

Preprints (www.preprints.org) | NOT PEER-REVIEWED | Posted: 26 June 2019 doi:10.20944/preprints201906.0257.v1

acquired and classified into different coordinate grids, which is discretized with a 5° latitude and 30° longitude spacing. That is, both of MLS and ACE-FTS dataset are classified by a monthly and geolocation grid. A diagram of constructing the integrated atmospheric profiles is shown in Figure 7.

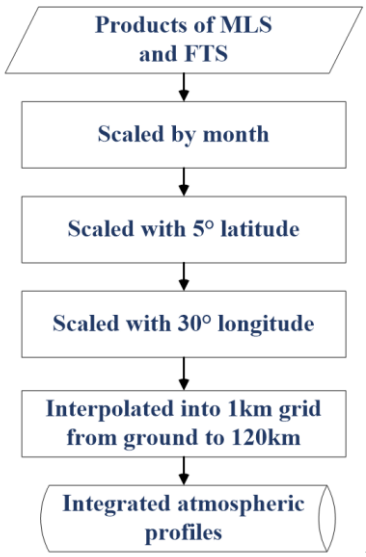

Figure 7 Process of constructing the integrated atmospheric profiles

The next step is to combine the two sets of profiles. Since ACE-FTS and AIUS have similar instrument characteristics, the ACE-FTS product is chosen in case that the profile of a particular species at the same geolocation and time can be found in both ACE-FTS and MLS datasets. Finally, profiles of the missing species are read from the AFGL dataset. The species profiles imported from AFGL dataset include NH_3, HBr, HI, PH_3, H_2S, F11, F12, F13, F21, F22, F114, F115 and HNO_4. These species profiles from FASCOD (Fast Atmospheric Signature Code) Model 1-6 are resampled and packed into the monthly geographic grids. In the end, the integrated atmospheric profiles dataset is produced.

4. Retrieval from AIUS measurements

4.1 Assessment of retrieval algorithm

Before performing the retrievals for AIUS measurements, the retrieval experiments are carried out based on simulated spectra and ACE-FTS measurement to test and verify our algorithm. Although no detailed parameterization of ACE-FTS instrument, the parameters of AIUS are adopted to perform retrieval experiments since the two instruments characteristic are similar. We adopt three ACE-FTS level 1 data to perform the O_3 retrieval experiments. Information of the ACE-FTS level-1 data used in this study is listed in Table 2. All the a prior profiles of O_3 and other species are taken from the dataset of integrated atmospheric profiles.

Table 2 Information of ACE-FTS Level 1 products

Data ID	Latitude [°]	Longitude [°]	date
43544	63	75	2011-9-14
38154	63	-73	2010-9-13
43611	70	-119	2011-9-18

Preprints (www.preprints.org) | NOT PEER-REVIEWED | Posted: 26 June 2019 doi:10.20944/preprints201906.0257.v1

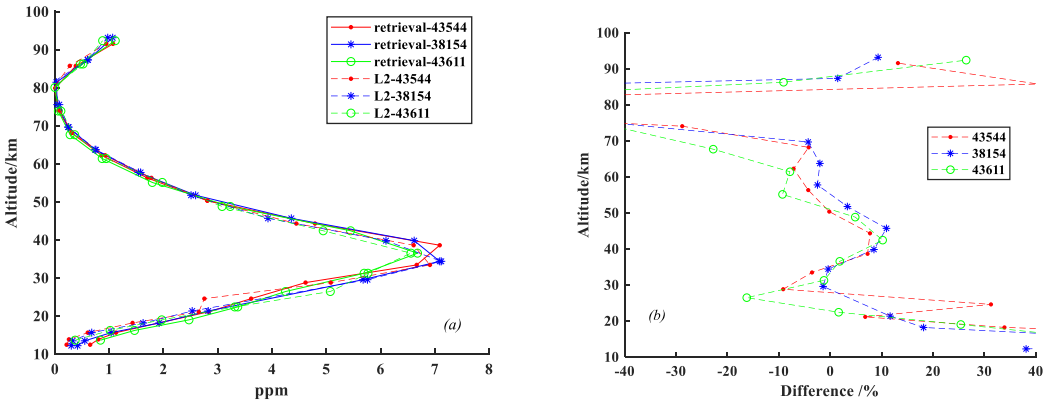

Figure 8 O_3 retrieval experiment based on FTS observation spectra. (a)Retrieval and ACE-FTS L2 profiles; (b) Relative difference between retrieval and FTS L2 products.

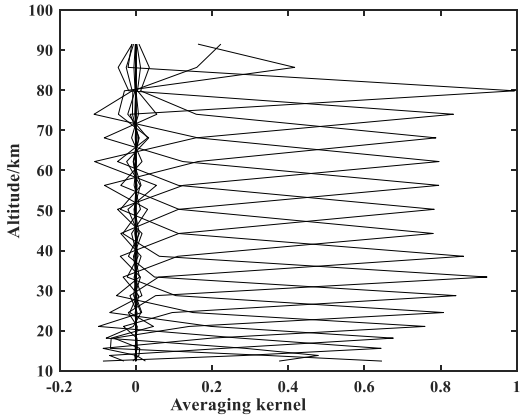

Figure 9 Typical averaging kernel for ACE-FTS O_3 retrieval

The retrieval profiles and the relative difference are shown in Figure 8. The solid lines represent O_3 retrieved by our algorithm and the dotted lines are ACE-FTS O_3 products which are resampled to the retrieval grid. The retrieval profiles presented in Figure 8(a) show that the shape of the retrieval O_3 profiles agree well to those of ACE-FTS level 2 products. The relative difference in Figure 8(b) illustrates that the relative difference of these three retrieval experiment is mostly within 10% between 20 km and 70 km for every pair of profiles, with some points reach 15%-30%. The relative difference is larger below 20 km and over 70 km because of the uncertainties in the measurements. The use of AIUS instrument parameterization may also contribute to the uncertainties of retrieval profiles. The bias of the ACE-FTS O_3 products is 1-8% in the stratosphere (16–44 km) and reaches up to 40% (20% on average) above 45 km [32-33]. The corresponding averaging kernels are plotted in Figure 9, which reveals that the retrieval information mainly comes from the measurement in the stratosphere. These retrieval experiments demonstrate that our retrieval algorithm performs stable and delivers comparable results using ACE-FTS measurement spectra.

4.2 Retrieval from AIUS

AIUS observes in a forward direction and scans one sequence (measurements from the lowest to the highest tangent altitudes) from one orbit. In this study, eight orbits measurements are used to perform O_3, H_2O and HCl retrieval experiments. The information of the 8 orbit level 1 data and the retrieval configuration are presented in Table 3 and 4.

The retrieval profiles of AIUS are compared with the official AURA/MLS level-2 v4.2 profiles. All MLS profiles for comparisons were chosen according to their quality and convergence flags. In

Preprints (www.preprints.org) | NOT PEER-REVIEWED | Posted: 26 June 2019 doi:10.20944/preprints201906.0257.v1

our retrieval configuration, the retrieval grid is the same as the observation grid. Thus, the retrieval grids are different for these eight measurements. Presently, the effective altitudes of AIUS measurements are about from 12 to 90 km. For comparison of mean profiles, both the retrieved AIUS and MLS profiles are resampled to the same altitude grids, from 12 km to 90 km with 2 km step below 30 km and 3 km step over 30km.

Table 3 Information of AIUS Level 1 products

Orbit ID	Latitude [°]	Longitude [°]	date
003301	-63	-76	2018-12-21
003364	-62.8	170.5	2018-12-25
003367	-62.8	96.4	2018-12-25
003369	-62.8	46.9°	2018-12-25
003372	-62.9	-27.3	2018-12-26
003458	-63.5	6.9	2019-01-01
003504	-64	-50	2019-01-04
003566	-64.7	-142.5	2019-01-08

Table 4 Retrieval configuration

Parameters	Retrieval configuration
Spectroscopic database	Hitran 2016 [34]
Continua used	O_2, H_2O, N_2 [35-37]
Retrieval altitude grids /km	Observation grids
Altitude grids in the forward model	0-100 km with 1 km spacing
The a prior profile	Integrated atmospheric database

4.2.1. O_3 retrieval

O_3 profiles are retrieved from the AIUS measurement spectra listed in Table 3 and compared to MLS O_3 profiles. Figure 11 shows a typical O_3 retrieval example based on AIUS measurements. MLS O_3 profiles used for comparison are the v4.2 datasets. According to the data quality document [38] and validation of O_3 product version 2.2 [39], the uncertainties of MLS O_3 profiles in the stratosphere are often about 5%-10%, but over 20% when the atmospheric pressure is < 0.1 hPa.

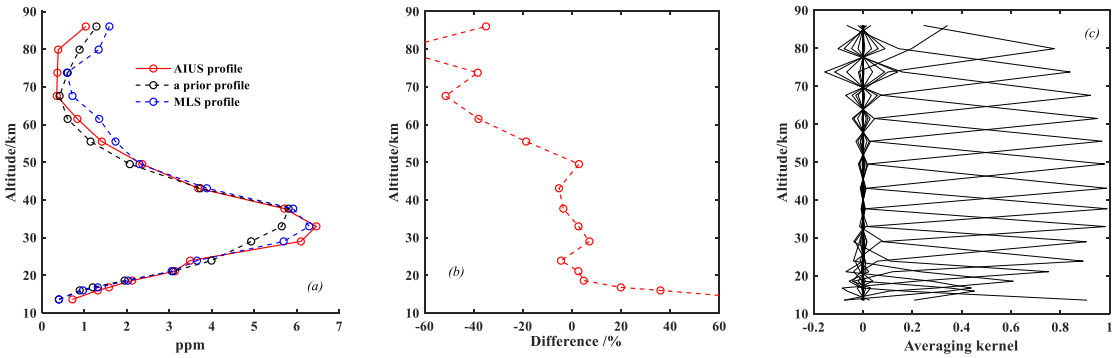

Figure 10 O_3 retrieval from AIUS measurement on orbit 003301. (a)Retrieval, the a prior and MLS L2 profiles; (b) Relative difference between retrieval and MLS L2 profiles; (c) Averaging kernel

From orbit 003301 measurement, the O_3 profile is retrieved between 12 km and 90 km. The retrieval AIUS O_3 profile is presented by red line, the a prior is black line and the MLS profile is the blue line, which is resampled to the retrieval grid. Figure 10 (a) show that the retrieval AIUS O_3

Preprints (www.preprints.org) | NOT PEER-REVIEWED | Posted: 26 June 2019 doi:10.20944/preprints201906.0257.v1

profile is obviously different from the a prior and agree rather well to the MLS O_3 profile in the stratosphere. The relative difference between the retrieval and MLS O_3 product in the Figure 10 (b) illustrates that the relative difference is 3-8% between 18 and 50 km, 20-40% at 15-20 km and mostly 20-40% from 55 km to 90 km with occasionally greater than 40%. Figure 10 (c) is the retrieval averaging kernel for orbit 003301 retrieval. The kernel reaches about 0.8-1 at 20-80 km, which mean the retrieval information mainly comes from the measurements.

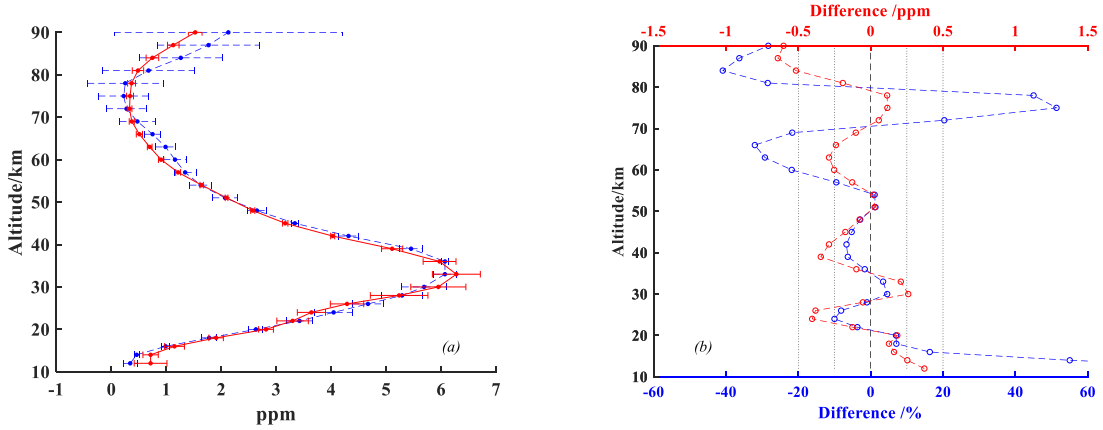

Figure 11 AIUS and MLS comparison for O_3 profiles. (a) Mean O_3 profiles and stander deviations of AIUS and MLS profiles, red for AIUS and blue for MLS; (b) Relative and absolute difference of mean O_3 profiles between AIUS and MLS, red for absolute difference and blue for relative difference.

O_3 profiles from AIUS measurements in Table 3 are retrieved. Since these measurements were all acquired near 65°S and in about 20 days, the comparison is made for the mean profile of the eight pairs of AIUS and MLS measurements. Figure 11 (a) shows the mean profiles from AIUS and MLS with the corresponding the standard deviations, which are showed by error bars. The standard deviations of AIUS profiles reach 0.45 ppm between 30 and 40 km, which are bigger than those of MLS profiles. This is because the two AIUS profiles retrieved from orbits 003504 and 003566 have lower peak values. The relative difference and absolute difference of the mean profiles of AIUS and MLS are presented in Figure 11 (b). It indicates that the relative difference is within 10% (about 0.02 - 0.4 ppm) between 18 and 58 km, 20-40% for 60-70 km and 80-90 km, about 15% for 15-20 km.

4.2.2. H_2O retrieval

The H_2O profiles are also retrieved from AIUS measurements in Table 3 and compared with MLS H_2O v4.2 profiles. For MLS H_2O v4.2 profiles, the accuracy is within 10% between 100hPa and 0.1hPa [38]. An example of H_2O retrieval is presented in Figure 12.

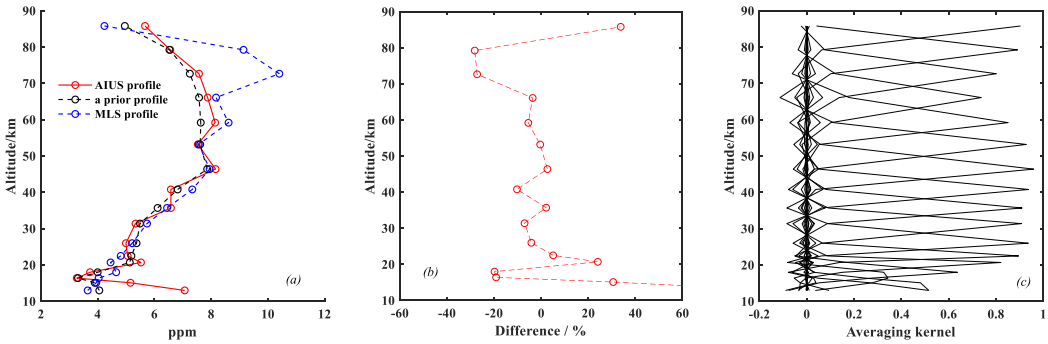

Figure 12 H_2O retrieval from AIUS measurement on orbit 003367. (a)AIUS profile, the a prior and MLS L2 profile; (b) Relative difference between retrieval and MLS L2 products; (c) Averaging kernel

Preprints (www.preprints.org) | NOT PEER-REVIEWED | Posted: 26 June 2019 doi:10.20944/preprints201906.0257.v1

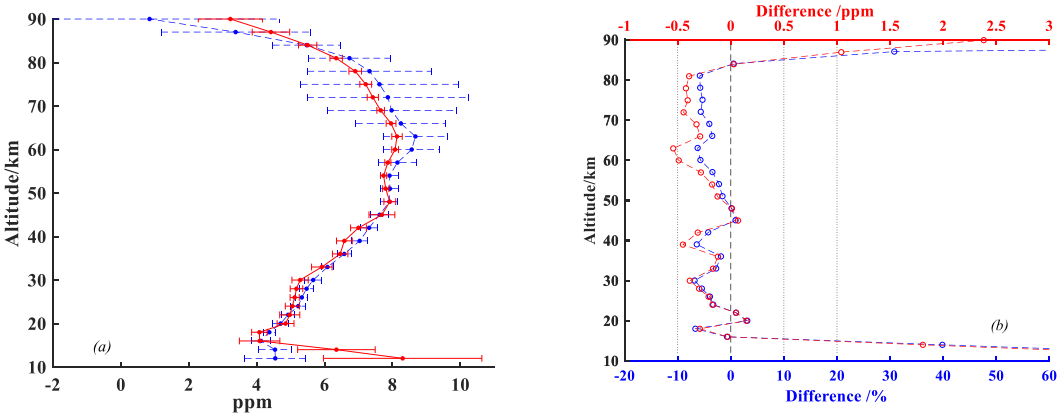

Figure 13 AIUS and MLS comparison for H_2O profiles. (a) Mean H_2O profiles and stander deviations of AIUS and MLS, red for AIUS and blue for MLS; (b) Relative and absolute difference of mean H_2O profiles between AIUS and MLS, red for absolute difference and blue for relative difference.

Figure 12 (a) shows the AIUS H_2O profile, the a prior and MLS H_2O profiles. The retrieval AIUS profile has large deviation from MLS profile between 70 and 80km, since the MLS profile have a sudden increasing there. For this pair measurement, the relative difference is mostly with 10% between 20 and 70 km, as can be seen from Figure 12(b). The averaging kernel in Figure 12(c) indicates that the AIUS retrieval is mostly based on the measurement information, not the a priori itself. The comparison of mean H_2O profiles between AIUS and MLS is shown in Figure 13. Only seven pairs of AIUS and MLS profiles are used to make comparison, because the quality of MLS profile from January 8, 2019 is less than the quality threshold. The mean AIUS H_2O profile has a rather good agreement with the mean MLS profile. The stander deviation of AIUS profiles is greater than that of MLS profiles below 20 km, while it is smaller between 70 and 90 km. Figure 13 (b) presents the absolute and relative difference between AIUS and MLS profiles. AIUS profiles mainly have a negative deviation from MLS profiles. The relative difference is within 10% (0-0.5 ppm) between 15 and 80 km. However, the relative difference can reach 20-50 % above 80 km and below 15 km.

4.2.3. HCl retrieval

The following Figures 14 and 15 present a typical HCl retrieval and the comparison of mean HCl profiles between AIUS and MLS. It has been reported that the accuracy of the MLS HCl v4.2 profiles is about 10% between 20 hPa and 0.32 hPa, and 10% - 40 % (occasionally more than 40%) between 100 hPa and 46 hPa [38].

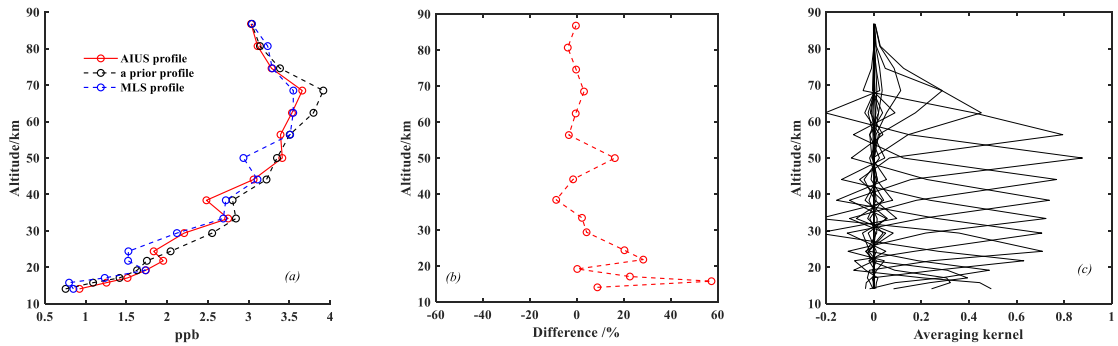

Figure 14 HCl retrieval from AIUS measurement on orbit 003458. (a) AIUS profile, the a prior and MLS L2 profile; (b) Relative difference between retrieval and MLS L2 products; (c) Averaging kernel

Preprints (www.preprints.org) | NOT PEER-REVIEWED | Posted: 26 June 2019 doi:10.20944/preprints201906.0257.v1

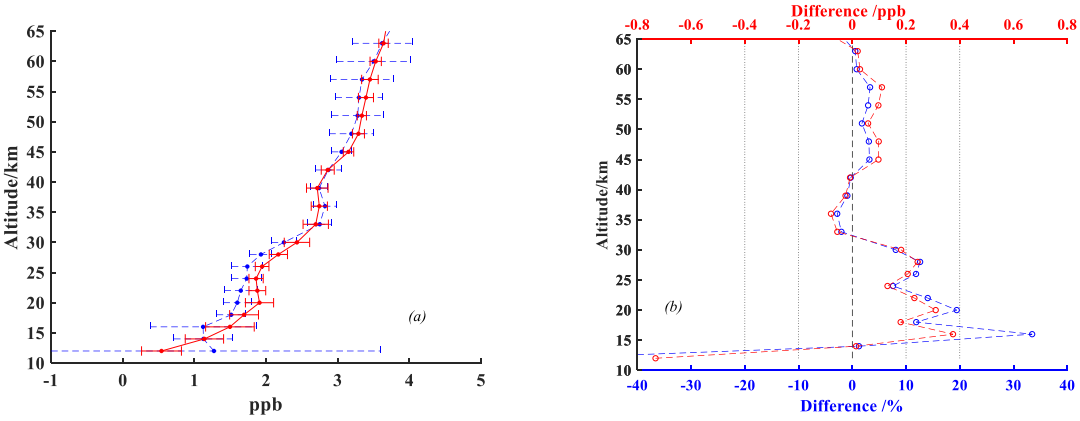

Figure 15 AIUS and MLS comparison for HCl profiles. (a) Mean HCl profiles and stander deviations of AIUS and MLS, red for AIUS and blue for MLS; (b) Relative and absolute difference of mean HCl profiles between AIUS and MLS, red for absolute difference and blue for relative difference.

The AIUS and MLS HCl profiles in Figure 14(a) capture the similar pattern. The relative difference in Figure 14(b) illustrates that the difference is almost within 10% between 20 and 90 km, except three points, which reach about 20%. The averaging kernel below 65 km is about 0.5-0.8. However it becomes rather smaller over 65 km, which means that the retrieval information mainly comes from the a prior. It is also reported by the data quality document that MLS HCl profiles is unsuitable for scientific use over 0.22 hPa [38]. Therefore, the comparison is made between 12 and 60 km (near 0.22 hPa). Figure 15(a) shows the mean HCl profile and stander deviations of AIUS and MLS. The stander deviations are presented as error bars. The HCl profiles from two instruments agree quite well. The stander deviations of AIUS profiles (red solid line) become bigger below 20 km, while they are smaller at other altitudes. Figure 15 (b) reveals that the relative difference is within 10% (about 0.1 ppb) between 30 and 60 km, and is about 10-20% (about 0.2 -0.4 ppb) between 16 and 30 km.

5. Discussion and conclusions

This study has introduced a retrieval algorithm developed for an infrared occultation spectrometer called AIUS, which is on-board the Chinese GaoFen-5 satellite. For the first time, O_3, H_2O and HCl profiles were retrieved from AIUS observation spectra, and the retrieved profiles were compared with the official AURA/MLS Level-2 products. Before performing retrieval for AIUS measurement, the retrieval experiments were carried out to assess our retrieval algorithm based on ACE-FTS measurements. The experiments demonstrate that the retrieval algorithm is reliable and work fine.

O_3, H_2O and HCl retrievals were performed using AIUS eight orbits measurements. The comparisons between AIUS and MLS indicate that the relative difference is within 10% between 18 and 58 km for O_3 profiles, within 10% between 15 and 80 km for H_2O profiles, within 10% between 30 and 60 km and 10-20% between 16 and 30 km for HCl profiles.

In the comparisons, lager differences of can be mostly found below 20 km and above 60 km. One possible reason would be that both retrievals are insensitive to the measurement information and rely on more on the a priori profile. Another possibility can be the quality of the AIUS measurements since the current level 1 processing still require further improvement.

In Our future work, the retrieval algorithm will be improved and more trace gases will be retrieved. In addition, an extensive retrieval error characterization will be analyzed. Further validations will be performed by comparing with MLS and other datasets using large amount measurement spectra during different periods and in different latitude bins.

Author Contributions: Xiaoying Li, Tianhai Cheng and Jian Xu conceived and designed the experiments; Hongmei Wang, Qi Luo, Songyan Zhu and Jing Miao performed the experiments; Xiaoying Li, Tianhai Cheng, Jian Xu, Hailiang Shi, Pengmei Xu, Xingying Zhang and Shule Ge analyzed the data; Xiaoying Li wrote the paper.

Funding: This research was funded by by National Natural Science Foundation of China under Grant 41571345, the National Key Research and Development Program of China under Grant 2016YFB0500705 and the Major Projects of High Resolution Earth Observation System under Grant 32-Y20A18-9001-15-17-1.

Acknowledgments: This study was supported in part by National Natural Science Foundation of China under Grant 41571345, the National Key Research and Development Program of China under Grant 2016YFB0500705, and the Major Projects of High Resolution Earth Observation System under Grant 32-Y20A18-9001-15-17-1. The ACE-FTS data were provided by ACE-FTS team. ACE, also known as SCISAT, is a Canadian-led mission mainly supported by the Canadian Space Agency (CSA). And Thanks to Professor Anu Dudhia for providing the RFM source code and help.

References

1. Manney, G.L.; Santee, M.L.; Livesey, N.J.; Froidevaux, L.; Read, W.G.; Pumphrey, H.C.; Waters, J.W.; Pawson, S. EOS Microwave Limb Sounder observation of the Antarctic polar vortex breakup in 2004. *Geophysical Research Letters*. **2005**, *32(L12811)*, 1-5, DOI: 10.1029/2005GL022823.
2. Santee, M.L.; Manney, G.L.; Livesey, N.J.; Froidevaux, L.; MacKenzie, I.A.; Pumphrey, H.C.; Read, W.G.; Schwartz, M.J.; Waters, J.W.; Harwood, R.S. Polar processing and development of the 2004 Antarctic ozone hole: First results from MLS on Aura. *Geophysical Research Letters*. **2005**, *32(L12817)*, 1-4, DOI: 10.1029/2005GL022582.
3. Gattinger, R. L.; McDade, I. C.; Alfaro Suzan, A. L. ; Boone, C. D.; Walker, K.A.; Bernath, P.F.; Evans, W.F. J.; Degenstein, D.A.; Yee, J.-H.; Sheese, P.; Llewellyn, E. NO_2 air afterglow and O and NO densities from Odin-OSIRIS night and ACE-FTS sunset observations in the Antarctic MLT region. *Journal of Geophysical Research*. **2010**, *115 (D12)* , 1256-1268, DOI: 115. 10.1029/2009JD013205.
4. Russell, J.M.; Gordley, L.L.; Park, J.H.; Drayson, S.R.; Hesketh, W.D.; Cicerone, R.J.; Tuck, A.F.; Frederick, J.E.; Harries, J.E.; Crutzen, P.J. The Halogen Occultation Experiment. *Journal of Geophysical Research-Atmospheres*. **1993**, *98(D6)*, 10777-97.
5. Gunson, M.R.; Abbas, M.M.; Abrams, M.C.; Allen, M.; Brown, L.R.; Brown, T.L.; Chang, A.Y.; Goldman, A.; Irion, F.W.; Lowes, L.L.; Mahieu, E.; Manney, G.L.; Michelsen, H.A.; Newchurch, M.J.; Rinsland, C.P.; Salawitch, R.J.; Stiller, G.P.; Toon, G.C.; Yung, Y.L.; Zander, R. The Atmospheric Trace Molecule Spectroscopy (ATMOS) experiment: Deployment on the ATLAS Space Shuttle missions. *Geophysical Research Letters*. **1996**, *23(17)*, 2333-2336.
6. Bovensmann, H.; Burrows, J.P.; Buehwitz, M.; Frerick, J.; Noel, S.; Rozanov, V.V. SCIAMACHY: Mission Objectives and Measurement Modes. *Journal of the atmospheric sciences.* **1999**, *56(2)*, 127-150.
7. Beer, R.; Glavich, T.A.; Rider, D.M. Tropospheric emission spectrometer for the Earth Observing System's Aura Satellite. *Applied Optics*. **2001**, *40(15)*, 2356-67.
8. Bernath P.F.; McElroy C.T.; Abrams M.C.; Boone, C.D.; Butler, M.; Camy-Peyret, C.; Carleer, M.; Clerbaux, C.; Coheur, P.-F.; Colin, R.; DeCola, P.; DeMazie`re, M.; Drummond, J. R.; Dufour, D.; Evans, W. F. J.; Fast, H.; Fussen, D.; Gilbert, K.; Jennings, D.E.; Llewellyn, E. J.; Lowe, R.P.; Mahieu, E.; McConnell, J.C.; McHugh, M.; McLeod, S.D.; Michaud, R.; Midwinter, C.; Nassar, R.; Nichitiu, F.; Nowlan, C.; Rinsland, C.P.; Rochon, Y.J.; Rowlands, N.; Semeniuk, K.; Simon, P.; Skelton, R.; Sloan, J.J.; Soucy, M.-A.; Strong, K.; Tremblay, P.; Turnbull, D.; A. Walker, K. ; Walkty, I.;. Wardle, D.A; Wehrle, V.; Zander, R., Zou, J. Atmospheric Chemistry Experiment (ACE): Mission overview. *Geophysical Research Letters*. **2005**, 32, L15S01, doi:10.1029/2005GL022386.
9. Fischer, H.; Birk, M.; Blom, C.; Carli, B.; Carlotti, M.; Clarmann, T.von; Delbouille, L.; Dudhia, A.; Ehhalt, D.; Endemann, M.; Flaud, J.M.; Gessner, R.; Kleinert, A.; Koopman, R.; Langen, J.; Lopez-Puertas´, M.;

Mosner, P.; Nett, H.; Oelhaf, H.; Perron, G.; Remedios, J.; Ridolfi, M.; Stiller, G.; Zander, R.. MIPAS: an instrument for atmospheric and climate research. *Atmos Chem Phys*. **2008**, *8(8)*, 2151-88.

10. Dong, X., Xu P.M. and Hou, L.Z., 2018, Design and Implementation of Atmospheric Infrared Ultra-spectral Sounder, *Spacecraft* Recovery *& Remote Sensing*, 2018, 39(3): 29-37.
11. Bernath P.F., C.T. McElroy, M.C. Abrams, C.D. Boone, M. Butler, C. Camy-Peyret, M. Carleer, et al. 2005. "Atmospheric Chemistry Experiment (ACE): Mission overview". *Geophysical Research Letters* 32, L15S01. DOI:10.1029/2005GL022386.
12. Wang, H.M., Xiaoying Li, Jian Xu , Xingying Zhang, Shule Ge, Liangfu Chen, Yapeng Wang, Songyan Zhu, Jing Miao and Yidan Si . Assessment of Retrieved N2O, NO2, and HF Profiles from the Atmospheric Infrared Ultraspectral Sounder Based on Simulated Spectra. Sensors. 2018, 18 2209; doi:10.3390/s18072209.
13. Zhu, S.Y., Li, X.Y., Xu, J., Cheng, T.H., Zhang, X.Y., Wang, H.M., Wang, Y.P., Miao, J. 2019, Neural network aided fast pointing information determination approach for occultation payloads from in-flight measurements: Algorithm design and assessment, *Advances in Space Research*, 63(8):2323-2336.
14. Dudhia, A. The Reference Forward Model (RFM), 2017, Journal of Quantitative Spectroscopy and Radiative Transfer. 2017, 186: 243–253, doi:10.1016/ j.jqsrt.2016.06.018
15. Von Clarmann, T..; Hopfner, M.; Funke, B.; Lopez-Puertas, M.; Dudhia, A.; Jay, V.; Schreier, F.; Ridolfi, M.; Ceccherini, S.; Kerridge, B.J.; Reburn, J.; Siddans, R. Modelling of atmospheric mid-infrared radiative transfer: the AMIL2DA algorithm intercomparison experiment. *Journal of Quantitative Spectroscopy & Radiative Transfer*. **2003**, *78*, 381-407.
16. Rodgers, C.D. Retrieval of atmospheric temperature and composition from remote measurements of thermal radiation. *Reviews of Geophysics and Space Physics*. **1976**, *14(4)*, 609-624.
17. Urban, J.; Baron, P.; Lautie, N.; Schneider, N.; Dassas, K.; Ricaud, P.; de la Noë, J. Moliere (v5): a versatile forward- and inversion model for the millimeter and sub-millimeter wavelength range. *Journal of Quantitative Spectroscopy and Radiative Transfer*. **2004**, *83(3/4)*, 529-554, DOI: 10.1016/S0022-4073(03)00104-3.
18. Boone, C.D.; Nassar, R.; Walker, K.A.; Rochon, Y.; McLeod, S.D.; Rinsland, C.P.; Bernath, P.F. Retrievals for the atmospheric chemistry experiment Fourier-transform spectrometer. *Applied Optics*. 2005, *44(33)*, 7218-31.
19. Raspollini, P.; Belotti, C.; Burgess, A.; Carli1, B.; Carlotti, M.; Ceccherini, S.; Dinelli, B.M.; Dudhia, A.; Flaud, J.-M.; Funke, B.; Hopfner, M.; Lopez-Puertas, M.; Payne, V.; Piccolo, C.J.; Remedios, J.; Ridolfi, M.; Spang, R. MIPAS level 2 operational analysis. *Atmos. Chem. Phys*.**2006**, *6*, 5605–5630.
20. Livesey, N.J.; Snyder, W.V.; Read, W.G.; Wagner, P. A. Retrieval Algorithms for the EOS Microwave Limb Sounder (MLS). *IEEE Transactions on Geoscience and Remote Sensing*. **2006**, *44(5)*, 1144-1155.
21. Bowman, K.W.; Rodgers, C.D.; Kulawik, S.S.; Worden, J.; Sarkissian, E.; Osterman, G.; Steck, T.; Lou, M.; Eldering, A.; Shephard, M.; Worden, H.; Lampel, M.; Clough, S.; Brown, P.; Rinsland, C.; Gunson, M.; Beer, R. Tropospheric Emission Spectrometer: Retrieval Method and Error Analysis. *IEEE Transactions on Geoscience and Remote Sensing*. **2006**, *44(5)*, 1297-1307.
22. Takahashi, C.; Ochiai, S.; Suzuki, M. Operational retrieval algorithms for JEM/SMILES level 2 data processing system. *Journal of Quantitative Spectroscopy & Radiative Transfer*. **2010**, *111*, 160–173.
23. Rodgers, C.D. *Inverse Methods for Atmospheric Sounding: Theory and Practice, Series on Atmospheric Oceanic and Planetary Physics-Vol. 2*, World Scientific Publishing Co. Pte. Ltd: P O Box 128, Farrer Road, Singapore, 2000; pp. 92-93, ISBN: 981-02-2740-X.
24. Eriksson, P. Analysis and comparison of two linear regularization methods for passive atmospheric observations. *Journal of Geophysical Research*. **2000**, *105(D14)*, 18,157-18,167.
25. Doicu, A.; Schreier, F.; Hess, M. Iteratively regularized Gauss – Newton method for atmospheric remote sensing. *Computer Physics Communications*. **2002**, *148*, 214–26.
26. Steck, T. Methods for determining regularization for atmospheric retrieval problems. *Applied Optics*. **2002**, *41(9)*, 1788-1797.
27. Jiang, D.M.; Dong, C.H. A review of optimal algorithm for physical retrieval of atmospheric profile. *Advances in Earth Science*. **2010**, *25(2)*, 133-139.
28. Zou, M.M.; Chen, L.F.; Li, S.S.; Fan, M.; Tao, J.H.; Zhang, Y. An improved constraint method in optimal estimation of CO2 from GOSAT SWIR observations. *Science China Earth Sciences*. **2016**, DOI: 10.1007/s11430-015-0247-9.

29. Xu, J.; Schreier, F.; Doicu, A.; Trautmann, T. Assessment of Tikhonov-type regularization methods for solving atmospheric inverse problems. *Journal of Quantitative Spectroscopy & Radiative Transfer*. **2016**, *184*, 274–286.
30. Eriksson, P.; Jimeneza, C.; Buehler, S.A. Qpack, a general tool for instrument simulation and retrieval work. *Journal of Quantitative Spectroscopy & Radiative Transfer*. **2005**, *91*, 47-64.
31. Kuai, L.; Natraj, V.; Shia, R-L.; Miller, C.; Yung, Y.L. Channel selection using information content analysis: A case study of CO2 retrieval from near infrared measurements. *Journal of Quantitative Spectroscopy and Radiative Transfer*. **2010**, *111*, 1296-1304.
32. Jones, A.; Walker, K.A.; Jin, J.J.; Taylor, J.R.; Boone, C.D.; Bernath, P.F.; Brohede, S.; Manney, G.L.; McLeod, S.; Hughes, R.; Daffer, W.H. Technical Note: A trace gas climatology derived from the Atmospheric Chemistry Experiment Fourier Transform Spectrometer (ACE-FTS) data set. *Atmos. Chem. Phys.* **2012**, *12*, 5207-5220.
33. Dupuy, E.; Walker, K. A.; Kar, J.; Boone, C. D.; McElroy, C. T.; Bernath, P. F.; Drummond, J. R.; Skelton, R.; McLeod, S. D.; Hughes, R. C.; Nowlan, C. R.; Dufour, D. G.; Zou, J.; Nichitiu, F.; Strong, K.; Baron, P.; Bevilacqua, R. M.; Blumenstock, T.; Bodeker, G. E.; Borsdorff, T.; Bourassa, A. E.; Bovensmann, H.; Boyd, I. S.; Bracher, A.; Brogniez, C.; Burrows, J. P.; Catoire, V.; Ceccherini, S.; Chabrillat, S.; Christensen, T.; Coffey, M. T.; Cortesi, U.; Davies, J.; Clercq, C. De ; Degenstein, D. A.; Maziere `, M. De; Demoulin, P.; Dodion, J.; Firanski, B.; Fischer, H.; Forbes, G.; Froidevaux, L.; Fussen, D.; Gerard, P.; Godin-Beekmann, S.; Goutail, F.; Granville, J. ; Griffith, D.; Haley, C. S. ; Hannigan, J. W.; Hopfner, M.; Jin, J. J.; Jones, A.; Jones, N. B.; Jucks, K.; Kagawa, A.; Kasai, Y.; Kerzenmacher, T. E.; Kleinbohl, A.; Klekociuk, A.R.; Kramer, I.; Kullmann, H.; Kuttippurath, J.; Kyrola, E.; Lambert, J.-C.; Livesey, N.J.; Llewellyn, E.J.; Lloyd, N. D.; Mahieu, E.; Manney, G. L.; Marshall, B.T.; McConnell, J.C.; McCormick, M. P.; McDermid, I. S.; McHugh, M.; McLinden , C. A.; Mellqvist, J.; Mizutani, K.; Murayama, Y.; Murtagh, D. P.; Oelhaf, H.; Parrish, A.; Petelina, S. V.; Piccolo, C.; Pommereau, J.-P.; Randall, C. E.; Robert, C.; Roth, C.; Schneider, M.; Senten, C. ; Steck , T.; Strandberg, A.; Strawbridge, K. B.; Sussmann, R.; Swart, D. P. J.; Tarasick, D. W.; Taylor, J. R.; Tetard, C.; Thomason, L.W.; Thompson, A. M.; Tully, M. B.; Urban, J.; Vanhellemont, F.; Vigouroux, C.; Clarmann, T. von; Gathen, P. von der; Savigny, C. von; Waters, J. W.; Witte, J. C.; Wolff, M.; Zawodny, J. M. Validation of ozone measurements from the atmospheric Chemistry Experiment (ACE). *Atmos. Chem. Phys*. **2009,** *9*, 287-343.
34. Gordon, I.E.; Rothman, L.S.; Hill, C.; Kochanov, R.V.; Tan, Y.; Bernath, P.F.; Birk, M.; Boudon, V.; Campargue, A.; Chance, K.V.; Drouin, B.J.; Flaud, J.-M.; Gamache, R.R.; Hodges, J.T.; Jacquemart, D.; Perevalov, V.I.; Perrin, A.; Shine, K.P.; Smith, M.-A.H.; Tennyson, J.; Toon, G.C.; Tran, H.; Tyuterev, V.G.; Barbe, A.; Császár, A.G.; Devi, V.M.; Furtenbacher, T.; Harrison, J.J.; Hartmann, J.-M.; Jolly, A.; Johnson, T.J.; Karman, T.; Kleiner, I.; Kyuberis, A.A.; Loos, J.; Lyulin, O.M.; Massie, S.T.; Mikhailenko, S.N.; Moazzen-Ahmadi, N.; Müller, S.P.; Naumenko, O.V.; Nikitin, A.V.; Polyansky, O.L.; Rey, M.; Rotger, M.; Sharpe, S.W.; Sung, K.; Starikova, E.; Tashkun, S.A.; Vander Auwera, J.; Wagner, G.; Wilzewski, J.; Wcisło, P.; Yu, S.; Zak, E.J. The HITRAN2016 Molecular Spectroscopic Database. *Journal of Quantitative Spectroscopy and Radiative Transfer*. **2017**, *203*, 3-69. doi:10.1016/j.jqsrt.2017.06.038.]
35. Mlawer, E.J.; Payne, V.H.; Moncet, J.-L.; Delamere, J.S.; Alvarado, M.J.; Tobin, D.C. Development and recent evaluation of the MT-CKD model of continuum absorption. Philosophical Transactions of the Royal Society A: Mathematical, Physical and Engineering Sciences. **2012**, *370 (1968),*. 2520-2556, DOI: 10.1098/rsta.2011.0295.
36. Thibault, F.; Menoux, V.; Le Doucen, R.; Rosenmann, L.; Hartmann, J.-M.; Boulet, Ch. Infrared collision-induced absorption by O2 near 6.4 μm for atmospheric applications: measurements and empirical modeling. *Appl. Opt.* **1997**, *36*, 563-567.
37. Lafferty, W.J.; Solodov, A.M.; Weber, A.; Olson, W.B.; Hartmann, J.-M. Infrared collision-induced absorption by N2 near 4.3 μm for atmospheric applications: measurements and empirical modeling. *Appl. Opt.* **1996**, *35*, 5911-5917.
38. Livesey, N.J., Read, W G., Wagner P. A., Froidevaux L., Lambert A., Manney G.L., Mill´an Valle L.F., Pumphrey H.C., Santee M L., Schwartz M.J., Wang S.H., Fuller R. A., Jarnot R.F., Knosp B.W., Martinez E., 2016, Version 4.2x Level 2 data quality and description document. JPL D-33509 Rev. B.
39. Froidevaux, L.; Jiang, Y.B.; Lambert, A.; Livesey, N.J.; Read, W.G.; Waters, J.W.; Browell, E.V.; Hair, J.W.; Avery, M.A.; McGee, T.J.; et al. Validation of Aura Microwave Limb Sounder stratospheric ozone. measurements. J. Geophys. Res. Atmos. 2008, 113, doi:10.1029/2007JD008771.